Experiments in Fluids 30 (2001) 683–695 © Springer-Verlag 2001

Characteristics of the reaction zone in a combustor operating at mild combustion

İ. B. Özdemir, N. Peters

Abstract The aerodynamic, chemical and thermal aspects of the mild combustion process have been studied with emphasis on mixing rates, flue gas recirculation and strong shear produced by reactants supplied from discrete jets. Time-averaged and instantaneous structures of turbulent flow were examined by visualization and local measurements within a 5400 W burner operating with methane with an overall equivalence ratio varying from 0.8 to 1.2 and at non-premixed and premixed modes. The results showed that the entrainment of the flue gases into the fresh mixture was very important for the initiation and progress of the reaction, and occurred in two successive mechanisms. Initially, the flue gases were driven with the reverse flow towards the annular exit where, by Biot–Savart induction, they acquired some momentum from the supply streams provided at the center. The resulting mixing process in the close vicinity of the burner was less intermittent and this was evident in relatively lower values of the second order moments of the residence time distribution. Slightly downstream, the second order moments were, however, increased by large-scale turbulent fluctuations and this led to the enhancement of the mixing process and introduced some further intermittency. The latter entrainment mechanism caused the flue gases to partially encapsulate the discrete jets, which resulted in islands of flammable mixture surrounded by the inert gases. Hence, as the instantaneous OH radical visualizations revealed, the reaction was only initiated away from the burner and in disconnected regions where the Rayleigh pictures showed strong temperature gradients. As the distance from the nozzle increased further, the reaction seemed to follow local flow patterns in that it progressed radially outwards with large structures, which resulted in an increased space-averaged temperature. Furthermore, the residence time decreased away from the burner and the flame came close to extinction due to the high stretching rates of the large structures. However, the flue gases entrained up to this point increased the inert content of the fresh mixture with chemical time scales comparable to the time scales of the flow. This allowed the reactants to attain temperatures near to those of the flue gases and to ignite with a small temperature rise, which led to a much lower thermal NO formation. The results also showed that when the equivalence ratio of the non-premixed mixtures was increased, the region where the combustion took place was shifted away from the burner and extended further downstream towards the roof. In the case of premixed combustion, however, the reaction started and terminated earlier and was confined to regions in close proximity to the axis. The emissions of OH radical occurred rather patchily and in relatively high concentrations.

Received: 6 June 2000/Accepted: 28 October 2000

İ. B. Özdemir (✉)
Istanbul Technical University
School of Mechanical Engineering, Mechanics Division
Gümüşsuyu, 80191 Istanbul, Turkey

N. Peters
Institut für Technische Mechanik, RWTH Aachen
52056 Aachen, Germany

The first author is glad to acknowledge the Alexander von Humboldt Foundation for the research fellowship at the Institut für Technische Mechanik, RWTH Aachen.

1 Introduction

With the advent of environmental regulations, there has been a greater awareness of use of fossil fuels and the performance of combustion systems, in particular burners and enclosures (Bowman 1992; Chomiak et al. 1992). Within the last two decades *improved combustion* has been redefined with the purpose of limiting pollutant emissions and noise by introducing systems that are economically feasible to build and operate. Nevertheless, thermal efficiency is still of primary concern and, hence, preheating is used in many applications with high temperatures to regain the energy lost by exhaust gases (Hanby 1994; Tanaka 1995). However, the immediate drawback in these processes is the increased peak flame temperatures and related NO_x emissions (Flamme 1994; Milani 1994).

Among the mechanisms (Miller and Bowman 1989; Hayhurst and Lawrence 1992) used to form NO, the most prominent high temperature process for an oxygen and nitrogen reaction in a combustible air mixture is that of Zeldovich (1946). For this process, it may be sufficient for the reactants to remain for a few seconds at temperatures of around 1600 °C and this could be as low as a few milliseconds when temperatures reach 2000 °C or above (Wünning and Wünning 1997). Since these are the typical peak flame temperatures seen when there is preheating, the time duration of residence at points of high temperature is of particular importance. The methods to reduce NO emission are, therefore, based on schemes to reduce either peak flame temperature or the residence time and oxygen concentration in zones with high temperature (Garg 1994; Wood 1994). The extraction of heat by the

injection of steam or using cooling rods can achieve lower peak flame temperatures, but this results in incomplete reaction and increases the emission of CO (Teng and Huang 1996). It has become evident that increasing efficiency and at the same time decreasing the NO formation are contradicting requirements which prove to be difficult to overcome with classical approaches (Bell and Warren 1983). The main means of compliance remains through radical measures in the aerodynamics of burners and enclosures with control over mixing mechanisms and residence time. Towards this end, an attractive scheme is the staged combustion with staging performed on either the fuel (Smart and Morgan 1994) or air introduction (Spliethoff et al. 1996), but it requires sophisticated designs with increased capital investment. However recent studies, such as Mastorakos et al. (1993), have shown that flue gas recirculation is indeed the most successful scheme to reduce peak flame temperature and NO emission. In this method, instead of mixing inert exhaust gases directly into a flame, flue gases are introduced upstream as a third component and dilute the fresh fuel/air mixture. When the combustion flow in the enclosure is arranged as in a reverse flow reactor (Mansour et al. 1989), the flue gas recirculation is achieved with the interior aerodynamics and this is called internal flue gas recirculation. The scheme can be applied with very high rates of flue gas recirculation and without costing efficiency.

The requirements for a stable flame for both non-premixed and premixed flames are closely associated with local flow and burning velocities, and mixture preparation. When flames are stabilized only by the flow conditions set by the burner, high peak flame temperatures in the combustion chamber cannot be avoided, particularly in the vicinity of the burner, which obviously increases the thermal NO formation. Furthermore, the combustion in natural gas burners becomes very unstable and noisy when chamber temperatures drop locally below 750 °C (Lang et al. 1987; McManus et al. 1993). However, if process temperatures can be raised above the self-ignition temperatures, the rate of flue gas recirculation that previously reached only 30% due to flammability limits (Zabetakis 1965) can be pushed up to a value as high as 100%. It is interesting to observe in these cases, as for example Fig. 1, that a stable combustion reaction can still occur even without a flame attached or stabilized in the vicinity of the burner (Flamme and Kremer 1995). The flame appears to lift off but the combustion reaction still continues further downstream with a quite diminished visibility that stems from a decrease in the radiation extending up to the ultraviolet range (Telger and Roth 1995). Apart from a change in the physical description of the flame, an immediate outcome is the reduction of burning intensity, resulting in a temperature rise limited to a few hundred degrees Kelvin. With the elimination of the adverse effects of preheating on the peak flame temperatures, the thermal NO formation is no longer a proviso for improving the thermal efficiency. Indeed, NO_x emission of the combustion without a visible flame can be as low as one-tenth of that with a visible flame (Wünning and Wünning 1997) and the noise is reduced by at least 10 dB. This mode of combustion has been called "mild combustion" by de Joannon et al. (1999). Plessing et al. (1998) have performed simultaneous laser-optical measurements of temperature and OH radicals in the reverse flow burner described by Wünning and Wünning (1997). Evaluating local events, they demonstrated that because of the small local heat

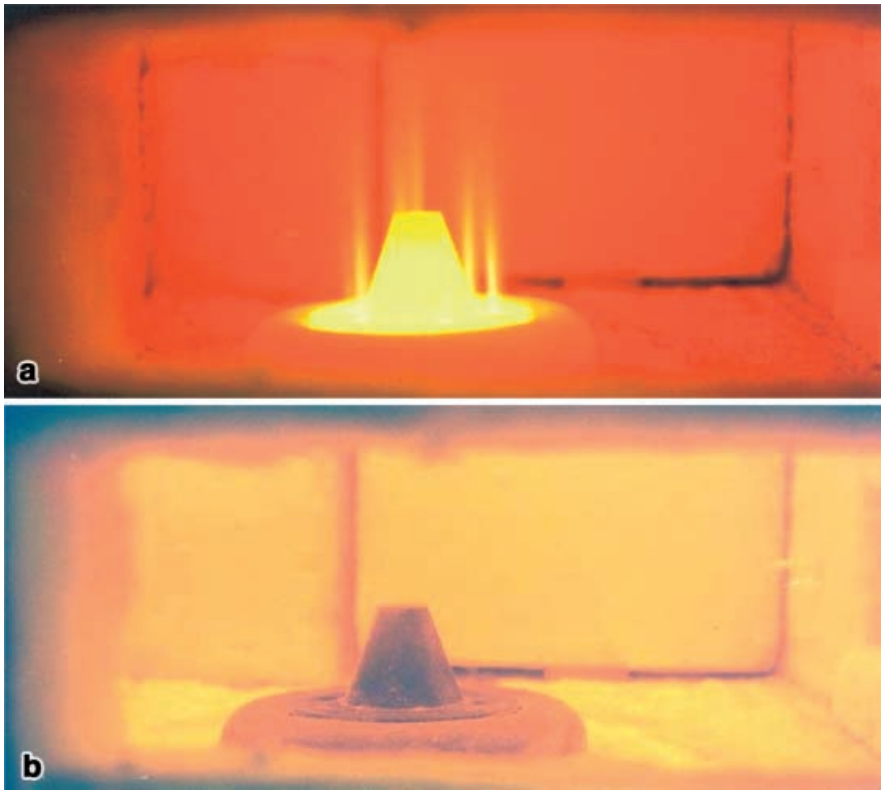

Fig. 1a, b. Visual observation of the region in the vicinity of the burner: **a** when the flames are visible and attached; **b** when the reaction occurs away from the burner so that the burner itself becomes relatively cooled

release the temperature difference between the highly preheated unburnt mixture and the burnt gas was so small that instead of the well-known S-shaped curve of temperature versus Damköhler number (Peters 2000), a monotonic dependence of the temperature on the Damköhler number existed. As a consequence, ignition and extinction phenomena cannot occur. This seems to be the most important physical characteristic of mild combustion and also explains the extremely silent operation of the burner.

The object of the present investigation was to study the mild combustion mode for both non-premixed and premixed mixture preparations. Aerodynamic, chemical and thermal descriptions of the mild combustion process were sought in a reverse flow type combustion chamber. The following section describes the flow configuration and measurement techniques, and results and discussion are presented in Sect. 3. The paper ends with concluding remarks and an appraisal of the physical interpretations to be used in engineering designs.

2
Flow configuration, measurement techniques and accuracy

The experimental arrangement of Fig. 2 comprised a multi-nozzle burner blowing vertically into an enclosure of 250×250 mm^2 cross-section and 485 mm length. The burner consisted of a central nozzle of 4.7 mm diameter, conically-elevated 25 mm from the six peripheral nozzles of 5 mm diameter located 40 mm away from the center. A 15.5-mm wide annular exit of 93 mm i.d. was located at the same side as the burner. The burner front surface was made of heat-resistant ceramic, and the steel enclosure was insulated internally by 50-mm thick material. The flow was optically accessible from three sides with five fused-silica glass windows of 100×85 mm^2 aperture with centers located at $z = 12.5$, 112.5, 212.5, 312.5, and 412.5 mm from the central nozzle at the bottom. The fuel was methane (CH_4) with a density of 0.668 kg/m^3 (at 20 °C and 1 atm), and the burner was run at 5,400 W with overall equivalence ratio, φ, varying from 0.8 to 1.2. The corresponding flow rates are listed in Table 1. In the non-premixed mode, the six peripheral nozzles supplied only the air with the fuel introduced from the central nozzle, whereas in premixed combustion, the central nozzle was unused with the air and fuel mixture being introduced peripherally. The wall temperature measured at a distance of $z = 112.5$ mm was around 1,040 °C and the temperature of the exhaust gases after exchanging heat with the incoming components was around 680 °C.

The axial and radial components of mean velocity, $\bar{U}_z$, and the auto- and cross-correlations of the corresponding fluctuations, u_z', u_r' and $\overline{u_z u_r}$, were measured with a laser Doppler velocimeter in the non-premixed combustion of $\varphi = 1$. The LDV system of Fig. 3a comprised a 800 mW argon–ion laser (Coherent Model Innova 300) with fiber optically coupled (Aerometrics FBD 140B) transmitting (Aerometrics XRV108) and receiving optics (Aerometrics RCV2108, RCM 2100LP). The flow was seeded with TiO_2 particles introduced into the burner from the air supply line. The particles were small enough (diameter < 3 μm) to follow the fluctuation of interest typically found in this kind of flows. The forward-scattered light was collected within a solid angle with axis 10 degrees to the transmitted laser beam to ensure high signal-to-noise ratio. With an effective frequency shift of 40 MHz, the signals were processed by an autocorrelation-based processor (Aerometrics RSA1000P) interfaced to a microcomputer. For each point, measurements were made with the beam plane oriented at −45, 0 and +45 degrees to the main flow direction. All velocity values were based on 2,500 individual measurements and, as a consequence, the average uncertainties in the mean and rms values of the velocity

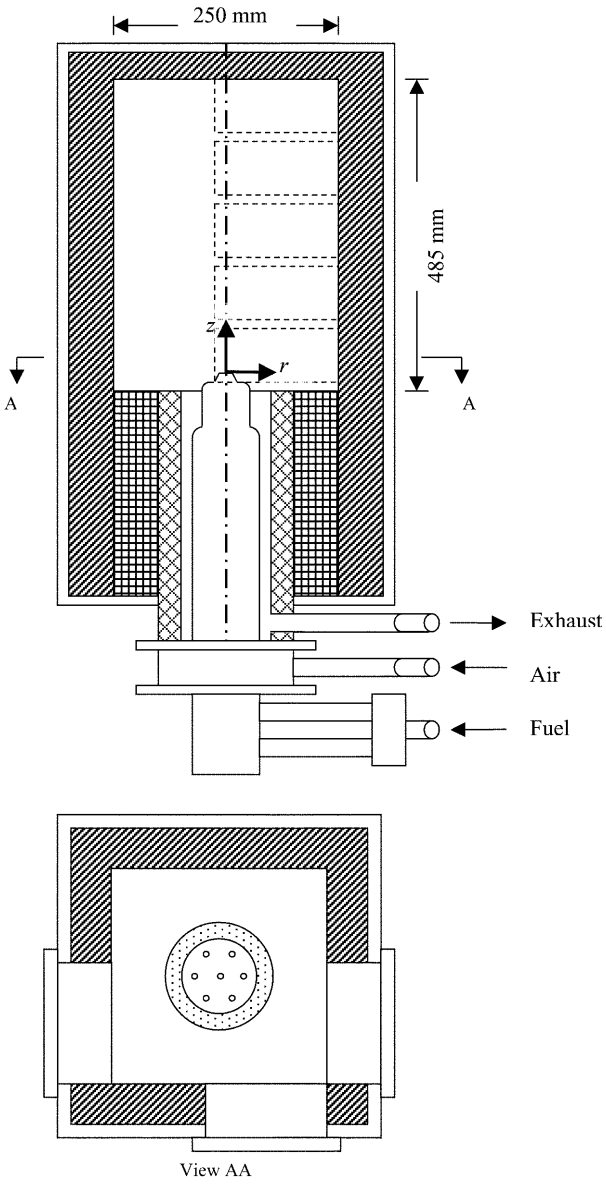

Fig. 2. The experimental arrangement comprising the multi-nozzle burner and the enclosure

Table 1. Fuel and air mass flow rates

F	m_{air} (kg/h)	m_{CH_4} (kg/h)
0.8	8.4	0.39
1	6.5	0.38
1.2	6.7	0.47

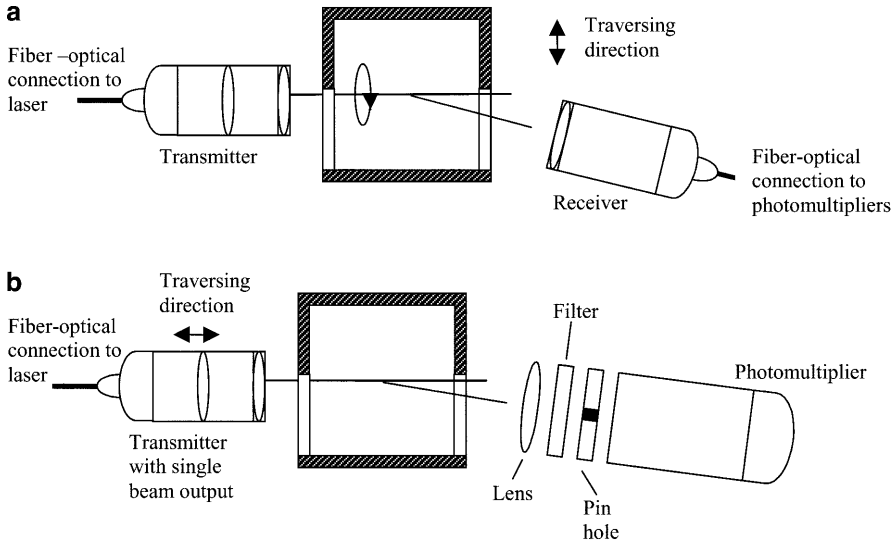

Fig. 3. Optical set-up for **a** LDV measurements; **b** Mie scattering

fluctuations (Yanta 1973) did not exceed 3% and 4% of the local values, respectively.

Information on local residence time within the enclosure was obtained from time-variations of the concentration of the passive tracer and was used to assess the efficiency of mixing in the non-premixed combustion of $\varphi = 1$. For this purpose, introduction of the tracer was suddenly stopped following a loading process, and remnants of passive tracer accumulated to that point were allowed to purge from steady state values. The unsteady sequence is called step-down procedure (Özdemir et al. 1996) and always produces smoother signals with continuous derivatives. The closure time of the passive tracer supply line was less than 0.1 s, which is considerably smaller than the time scales of the flow (3 s or more) so that a sharp fall in the concentration was assumed at the inlet. The local concentration values were inferred from the intensity of the light scattered by TiO_2 particles from a point on a 800 mW argon–ion laser beam (see Fig. 3b). Mie-scattered light, collected by a plano convex fused-silica lens of aperture 50 mm and focal length 120 mm, was filtered at the laser line by an interference filter (514IFS10) and focused onto a photomultiplier tube (Hamamatsu R1477). The receiving optics were aligned at 10 degrees to the transmitted laser beam. The measurement volume, truncated by a pin hole (600 μm), was around 0.8 mm long. Since no significant spatial variation of the distribution of particle size was expected, marker shot noise due to poly-dispersed particles, with larger particles scattering light more efficiently than small ones, would have only a negligible effect on the proportionality of concentration with light intensity. It has been known for some time (Long et al. 1981) that for large-scale mixing the difference in the mobility of the molecules and seed particles has only a minor effect on the concentration information inferred from scattered light. But it should also be pointed out that particles were still large enough for Brownian diffusion to be negligible.

Temperatures and OH radical concentrations were measured simultaneously by two-dimensional Rayleigh and laser induced predissociative fluorescence (LIPF) techniques, respectively. Figure 4 shows the general arrangement of the multi-point OH-LIPF and Rayleigh experiments. The illumination and excitation system comprised a pulsed KrF-excimer laser (Lambda Physics EMG 150 TMSC) with 250 mJ per pulse of 30 ns duration. The system was tuned between 247.9 nm and 248.9 nm with a line width of around 0.0001 nm. The output beam of rectangular cross-section (22×4 mm^2) was reflected by a mirror (DLHS UV248) into a polarizer plate (MgF_2) and then passed through a cylindrical lens of 1,200 mm focal length and a slit aperture to form a collimated vertical light sheet which crossed the burner through two opposing slit apertures of 2×40 mm^2 upon probing the combustion zone centrally. The windows were made with fused-silica glass to ensure maximum ultraviolet transmission, and the light reflected and emitted was collected at 90 degrees from the incident laser sheet in the region of interest of 30 mm wide and a fairly uniform thickness of 0.25 ± 0.03 mm.

A long-pass mirror (FLP2) positioned at an angle of 45 degrees reflected the scattering light at the excitation wavelength 248 nm towards camera 1 while letting the rest, including the OH emission, pass through in the direction of camera 2. The light collected by two plano convex fused-silica lenses of aperture 50 mm and equivalent focal length 81.8 mm was filtered at the Rayleigh line by an interference filter (250IFS10) and focused onto a 25 mm diameter DEP image intensifier of 30 lp/mm resolution, connected with an enhanced fiber optical coupling to a 16-bit 512×512 pixel CCD camera (LaVision). The temperatures were inferred from the distribution of light intensity recorded on Rayleigh images that were corrected for light intensity and detector non-uniformities and background noise. Since the emissivity of the insulating material inside the chamber walls was temperature dependent, the correction applied to the calibration frames (Long 1992) was different for the room temperature (23 °C) and higher temperatures. Background images were constructed at each location using the images of He and air with the chamber at room temperature and at a temperature depicting those typically found during the combustion. In order to obtain best estimate of the background during the combustion process, an iterative correction was

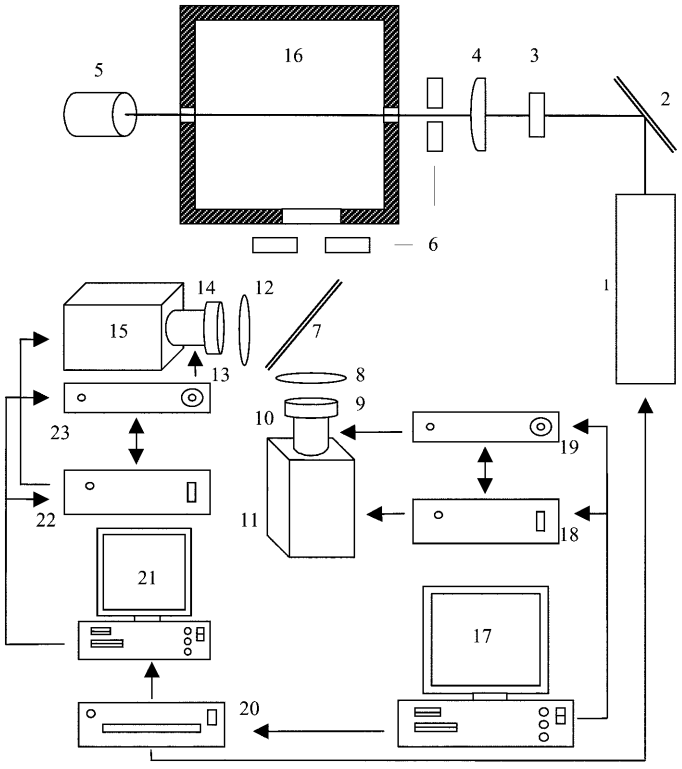

Fig. 4. General arrangement of the multi-point OH-LIPF and Rayleigh experiments

applied on the images taken at a temperature of about 950 °C. Once the images were corrected for background noise, then the intensity values were converted to temperatures using the relation (Stepowski 1992; Zhao and Hiroyasu 1993)

$$T = T_0(P/P_0)(\sigma_e/\sigma_{e0})(I_0 - I_{B0})/(I_R - I_{BR}) \ ,$$

where T_0 and P_0 are the standard ambient temperature and pressure, respectively (23 °C and 760 mmHg). The only unknown parameter in the above equation is the effective Rayleigh cross-section of the burning mixture defined as $\sigma_e = \Sigma X_i \sigma_i$, where X_i is the mole fraction of species i and σ_i is its Rayleigh cross-section. The mole fraction of the mixture is not known a priori due to the strong dilution with exhaust gases. The best estimate for σ_e would be obtained from the mole fraction of the reactants, assuming σ_e is changed negligibly between unburnt and burnt gases. The error introduced due to this assumption has been reported as less than 5% (Namer and Schefer 1985).

For OH-LIPF, the $P_2(8)$ line was chosen to excite from the $A^2\sigma^+ \leftarrow (X)^2\pi(3, 0)$ state as reported by Kohse-Höinghaus (1994). Behind the long-pass mirror, two plano-convex fused-silica lenses of aperture 50 mm and equivalent focal length 87.7 mm were used to image an area of about 25×35 mm^2. The light emitted by the excited OH radicals was separated at around 298 nm from broadband emissions by a glass filter (UG11) and focused onto an 18-mm diameter Varo image intensifier with a resolution of 20 lp/mm, which was a tandem lens coupled to a 12-bit 384×576-pixel CCD camera (Photometrics). The exposure time was 350 ns in order to suppress natural flame luminescence. No calibration attempt was made and, therefore, the results based on OH-LIPF images are only qualitative.

3
Discussion of results

In the following, the aerodynamic results are presented first for the non-premixed combustion with $\varphi = 1$, followed by those for OH concentration and temperature for the premixed and non-premixed combustion.

3.1
Velocity field

First- and second-order moments of two velocity components were examined to identify the streamlines transporting passive scalars and the effect of turbulent fluctuations on the kinematics of mixing within the region where the reaction was mainly taking place. Axial and radial components of the mean velocity, $\bar{U}_z$ and $\bar{U}_r$, were presented in Fig. 5 where the cylindrical coordinate system is aligned with the axis of the central jet. Just downstream the burner ($z = 12.5$ mm), the maximum axial velocity was as large as 32 m/s with the corresponding shear layer extending up to a distance of 10 mm on both sides of the exit. At large radial distances from the center, positive velocities were replaced with small negative velocities of the reverse flow. Since the flow was seeded with particles introduced from the air inlets, the fuel jet and the flow set in the neighborhood had not received enough passive markers up to this distance to be represented in the LDV measurements. At a slightly higher distance from the burner, the flow patterns of the fuel and five peripheral air jets quickly combined into a single jet of bell-cone shape with width extending up to 40 mm away from the centerline. It will become clear in the following that away from the burner, particularly in the region where the reaction was mainly taking place ($z = 312.5$ mm), the axial momentum was convected laterally with the expansion of hot

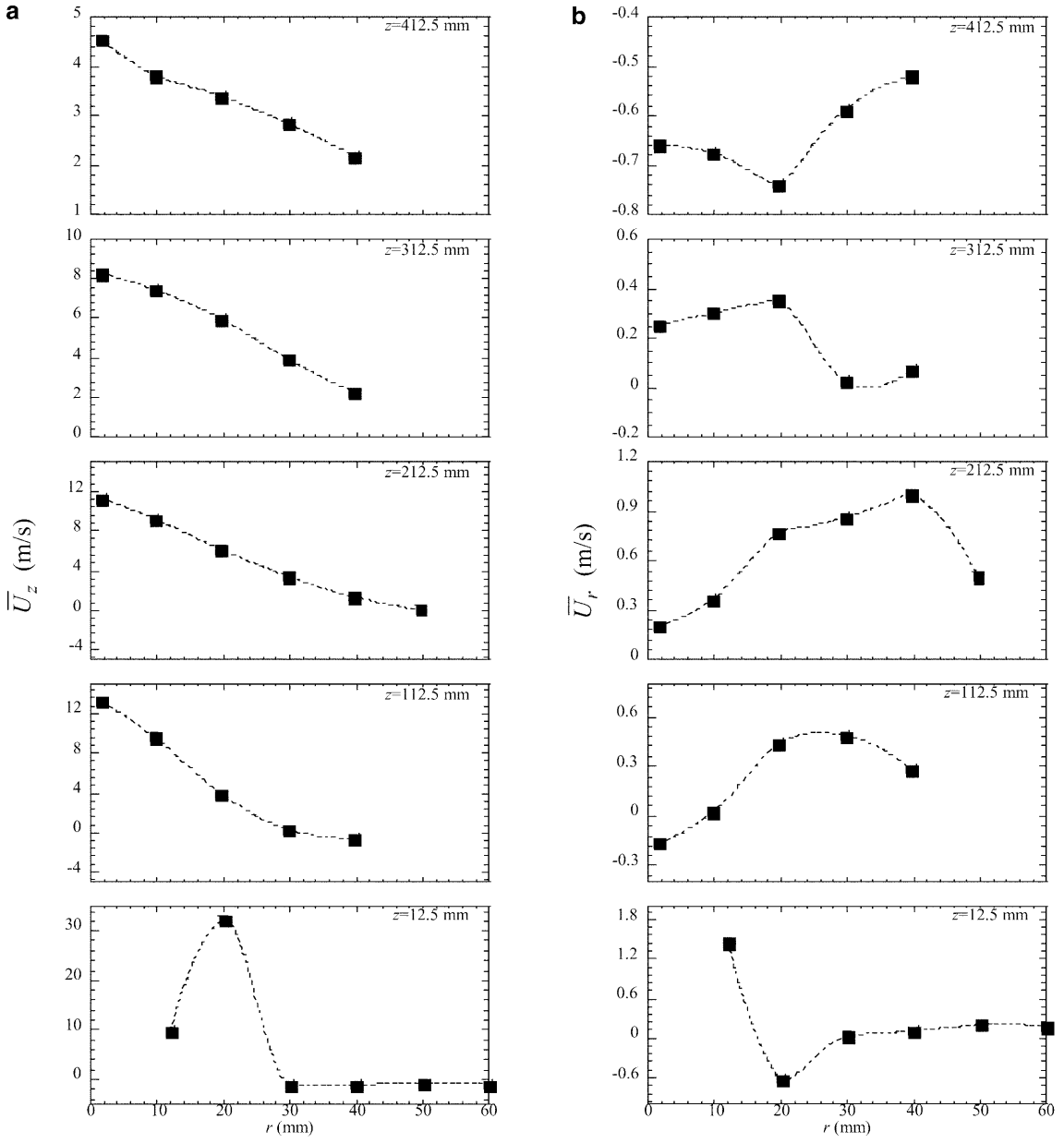

Fig. 5a, b. Time-averaged mean velocities in the vicinity of the burner axis: **a** axial component; **b** radial component

gases. This, however, occurred at the expense of maximum velocity, which was reduced to one-third with smoother gradients in the radial direction. As can be seen in Fig. 5b, the outward momentum of the peripheral air jets was opposed at large radial distances by the exhaust gases driven back to the vicinity of the burner. Therefore, low velocity values predominated in this region. On the other hand, the inward spreading of the air jets was prohibited around the centerline by the flow set by the fuel jet so that negative radial velocities appeared to be confined between $r = 16$ and 26 mm. The influence of the fuel jet decreased with the distance along the burner axis ($z = 112.5$ mm) and disappeared completely at $z = 212.5$ mm where the heat release due to the progress of the chemical reaction became dominant. Radial momentum at these axial locations, which seemed relatively small compared to the axial momentum, was generated by the thermal expansion of the hot gases rather than the spreading of the jets. The hot gases produced along the centerline pushed the peripheral air jets further away so that zero radial velocity was no longer located at the axis of the air jets and was displaced inwards. The peak values of the radial mean velocities at $z = 212.5$ mm gradually decreased and finally evolved into negative velocities of $z = 412.5$ mm, indicating a stagnation bubble for the flow decelerating against the roof the chamber.

Intensity of axial velocity fluctuations (u_z'), Fig. 6a, exhibited very high turbulence with peak values varying from 28% near the burner to 52% at the uppermost measuring location. Turbulent fluctuations were, however, higher in the absolute sense near the burner where the mixing effects were localized within the shear layers of the

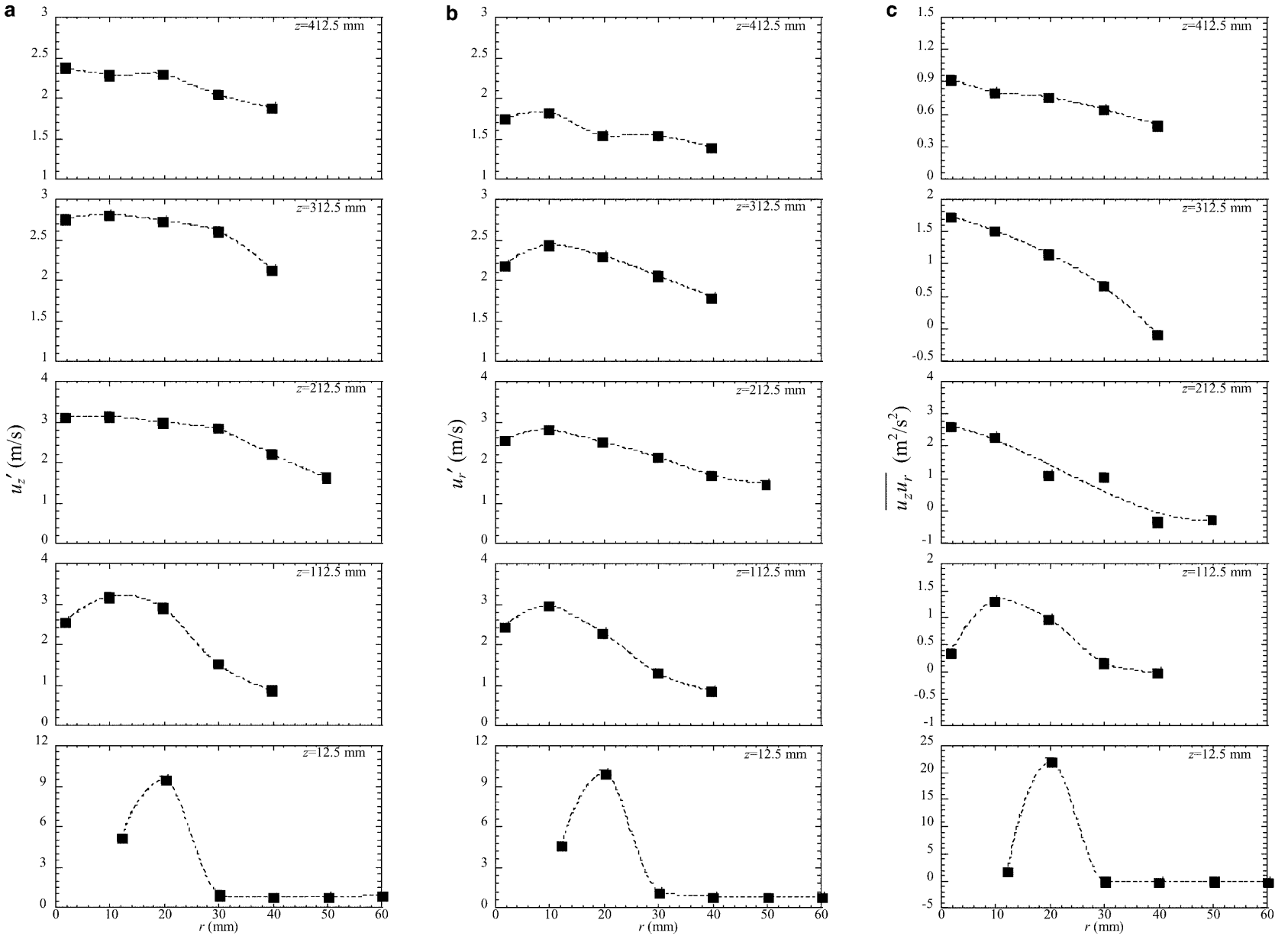

Fig. 6a–c. Time-averaged fluctuation velocities in the vicinity of the burner axis: **a** axial component; **b** radial component; **c** cross-correlation

air jets. It should also be pointed out that the measurement grid in the radial direction was not sufficient to resolve sharp gradients existing within the air jets so that the peak of the fluctuations in the shear layer might appear slightly outside the area where it was actually located. Further away from the burner, with the disappearance of the low velocities between the fuel and air jets, the flow developed a more uniform distribution of u'_z. The magnitudes of the radial velocity fluctuations (u'_r), Fig. 6b, were considerably higher than the corresponding mean values, and the profiles exhibited more structure that remained even far away from the burner. It was interesting that although the components of mean velocity in two orthogonal directions were quite different in magnitude and structure, their fluctuations had very close values and exhibited similar trends. Near the burner, cross-correlations of the velocity fluctuations, $\overline{u_z u_r}$, had large positive values within the air jets and were effectively zero elsewhere (see Fig. 6c). As the distance from the burner increased, the profile with a localized peak broadened with the tail extending radially outwards from the centerline. Although the correlation was in general positive, at the elevation $z = 212.5$ mm where a strong gradient of radial velocity existed, it attained relatively small negative values far away from the centerline. The trend of Reynolds stresses, which could be obtained from these profiles, generally agrees with the radial gradient of the axial velocity, as the momentum transport theorem would indicate.

The aerodynamic results presented so far describe high turbulent mixing rates and, thus, the fast chemistry assumption cannot be applied. This means that finite rate chemistry effects need to be considered. This has been done in a companion paper by Coelho and Peters (2001), where the Eulerian particle flamelet model was used to calculate combustion in this burner, in that residence time effects were found to control NO_x emissions. In an attempt to further discuss this matter, residence time scales are given in the next section, followed by OH emission and temperature results for different equivalence ratios.

3.2
Characteristics of the residence time

The probability density functions (pdf) of the residence time obtained from local concentration values of the passive marker exhibited a positively skewed distribution with tails extending towards large values of time, indicating that the population of passive scalar introduced at earlier times predominated. It is evident that the mixing between the fresh air and the flue gases recirculated back to the inlet plane broadens the pdf in the close vicinity of the burner. When the air jets combined into a single structure, the pdf became narrower at the locations between $z = 112.5$ and 212.5 mm. However, as the distance from the burner was further increased, the pdf again became wider particularly near the axis, revealing a recirculating motion set by the stagnation bubble of the flow approaching the roof of the chamber. Time scales associated with these distributions were quantified with the moments of Fig. 7. Mean values of the residence time (τ_1) immediately above the burner, Fig. 7a, were observed to be very high with a peak value of 11.3 s located between the fuel and air jets. It is evident that there exists a dead zone between the fuel and peripheral air jets wherein, when a passive scalar was introduced, it was trapped and stayed longer than anywhere in the flow domain. As the discrete air jets were combined ($z =$ 112.5 mm), τ_1 decreased along the burner axis nearly to one-third, though slightly larger values were still observed off-axis before eventually attaining a decreasing trend at large radial distances. Since flammability limits become closer by decreasing the residence time (Mansour et al. 1989), the flame is likely to be nearly extinct in this region. At slightly greater distances ($z = 212.5$ and 312.5 mm), the mean residence time stayed low within the mainstream near the axis and in the return flow far away, and was relatively higher elsewhere. Near the roof of the chamber, the mean residence time remained nearly constant with some scatter.

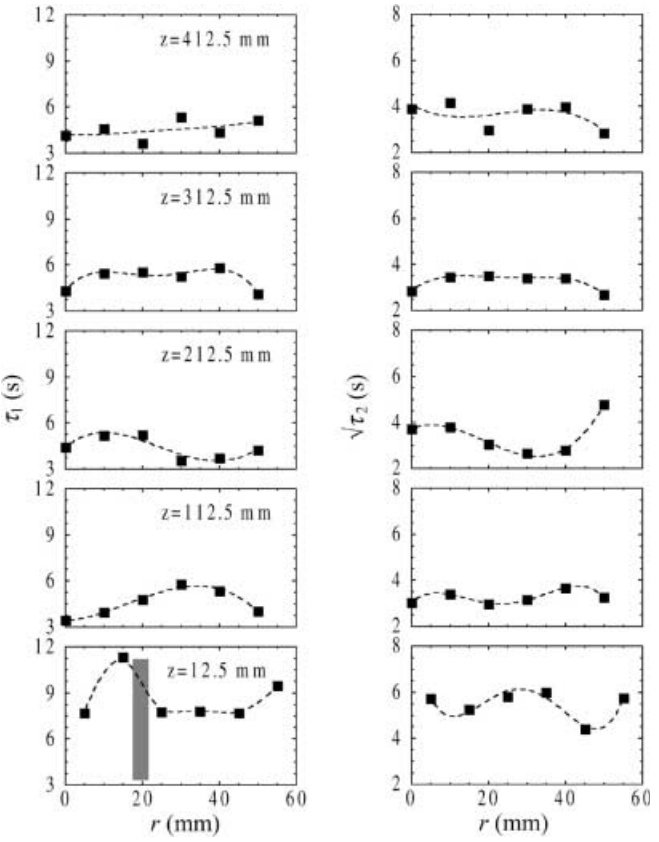

Fig. 7. Time scales associated with the residence time

The rms values of the residence time ($\sqrt{\tau_2}$) were shown in Fig. 7b where immediately above the burner, they can be seen as high as 6 s. This level first decreased with the distance from the burner, and then increased slightly towards the roof, especially when the mainstream separated from the burner axis to form a stagnation bubble. Considering the mean values, these levels present fairly high relative intensities, which reveal that the flow away from the burner particularly near the roof exhibited more intermittent characteristics (Perry et al. 1980) than anywhere else. Although there seemed quite a scatter in the data for higher order moments, non-zero values of the third order moments quantified the skewed character of the distributions and it

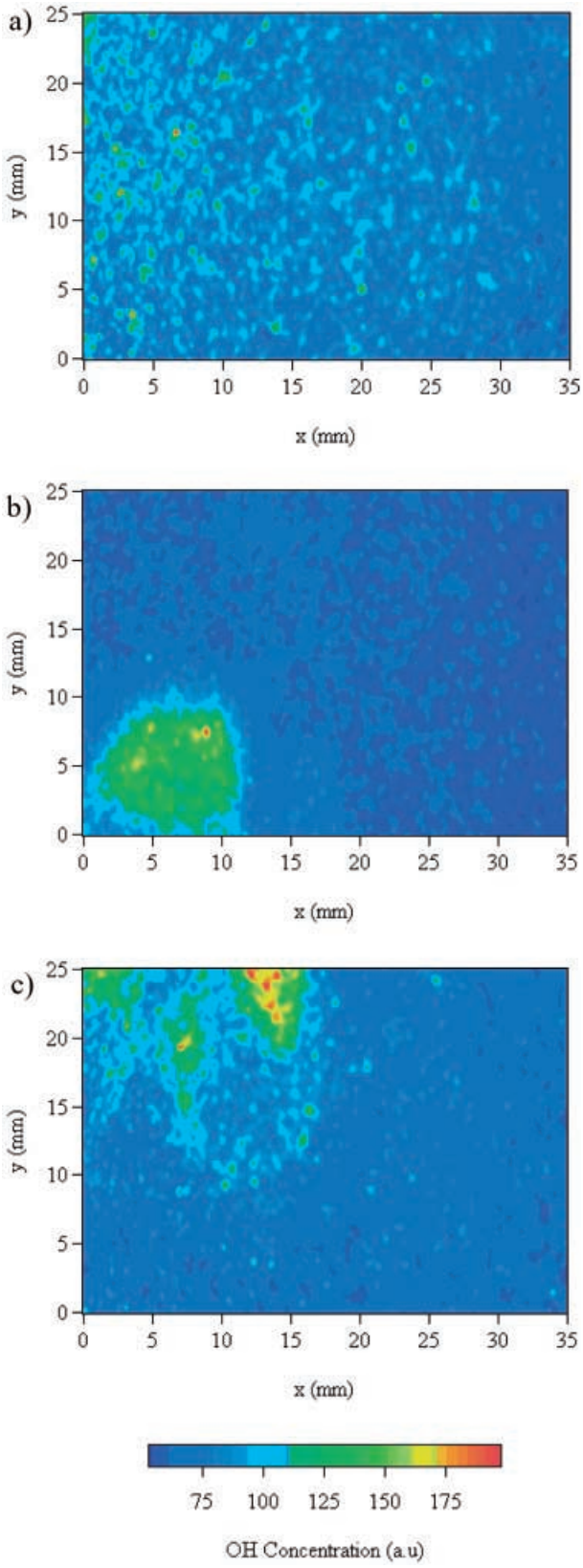

Fig. 8a–c. Instantaneous pictures of OH concentration for non-premixed combustion with $\varphi = 0.8$. **a** 4th window centered at $z = 312.5$ mm; **b** 3rd window centered at $z = 212.5$ mm; **c** 2nd window centered at $z = 112.5$ mm

was clear enough in the fourth order moments that the distributions were very different from a Gaussian profile.

3.3
OH concentrations and temperature field

Figures 8–10 show samples of instantaneous pictures of OH concentration and the corresponding temperature distributions in non-premixed combustion for equivalence ratios 0.8, 1, and 1.2, respectively. When the burner was run lean, Fig. 8, no OH was detected at either the first window just above the burner ($z = 12.5$ mm) or at the last window below the roof. It is evident that combustion occurred in a region from the upper part of the second window to the lower part of the third window and was confined to the close proximity of the axis. The reaction in this region manifested itself with the rather patchy appearance of OH radicals of high concentration. Relatively lower but evenly distributed values of OH concentration at the fourth window showed that the process was nearly terminated, and that the values were due to passively convected remnants of the combustion. Indeed, concentrations of OH radical for the lean combustion appeared lower than the values for higher equivalence ratios and indicated a relatively less intense reaction whose structures left no distinct thermal signature to be recognized by the Rayleigh process. When the equivalence ratio was increased to $\varphi = 1$, the region where the combustion took place was shifted axially further downstream towards the roof. For this case, there appeared no trace of OH radical in the first and second windows and, as Fig. 9 shows, the reaction started at the third window. As the distance increased, the reaction seemed to follow the local flow patterns which occasionally progressed radially outwards with large structures as for example the braid in Fig. 9b and, finally, filled the whole fifth window. The corresponding Rayleigh pictures revealed that in a small region near the burner axis, where the reaction was confined initially, strong temperature gradients prevailed. However, away from the burner these were replaced by smaller variations in that temperature rise due to reaction seemed limited to a few hundred degrees. When $\varphi = 1.2$ (Fig. 10) a very similar pattern as the $\varphi = 1$ case was observed. It is evident that for both $\varphi = 1$ and 1.2, the location corresponding to the fourth window appears to be the distance where the temperature gradient became the smoothest. The space-averaged temperature distribution, Fig. 11, revealed that it was also this location where the peak temperature occurred. The region was considered as the major reaction zone up to which the reactants were continuously heated by the mixing process with the flue gases. Therefore, the temperature rise due to the combustion was significantly lower than that of a typical combustion with a visible flame. The fact that the peak temperature occurred further downstream on the burner axis agrees well with the thermocouple measurements of Plessing et al. (1998). This can be attributed to the aerodynamics of the burner, which introduced hot flue gases upstream of the combustion region as a third component, suppressing reaction kinetics and so reducing burning intensity significantly. The combustion was sustained with

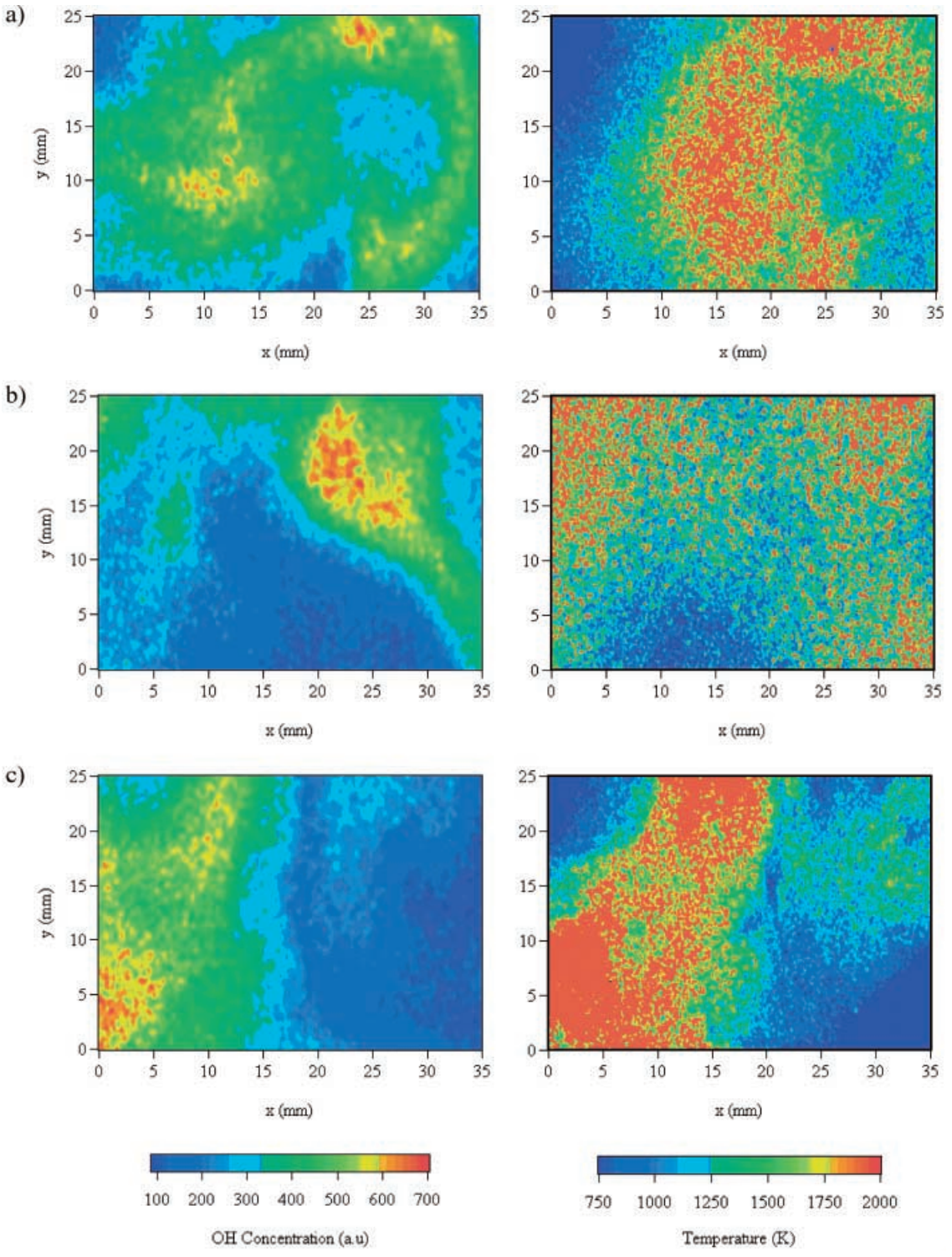

Fig. 9a–c. Instantaneous pictures of OH concentration and temperature for non-premixed combustion with $\varphi = 1.0$. **a** 5th window centered at $z = 412.5$ mm; **b** 4th window centered at $z = 312.5$ mm; **c** 3rd window centered at $z = 212.5$ mm

a strong flue gas recirculation, because space-averaged temperatures were still high for the reaction zone located far downstream from the burner. However, this would not be the case when a visible flame, stabilized near the burner, was lifted off. An immediate outcome of the smaller temperature difference between the reactants and the products should have been the lower NO_x emissions (Wünning and Wünning 1997).

The flow described in this study with high mixing rates and recirculation seems very suitable, for example, for gas turbine combustors where lean blow-out is a problem of great importance (Saul and Altemark 1991; McVey et al.

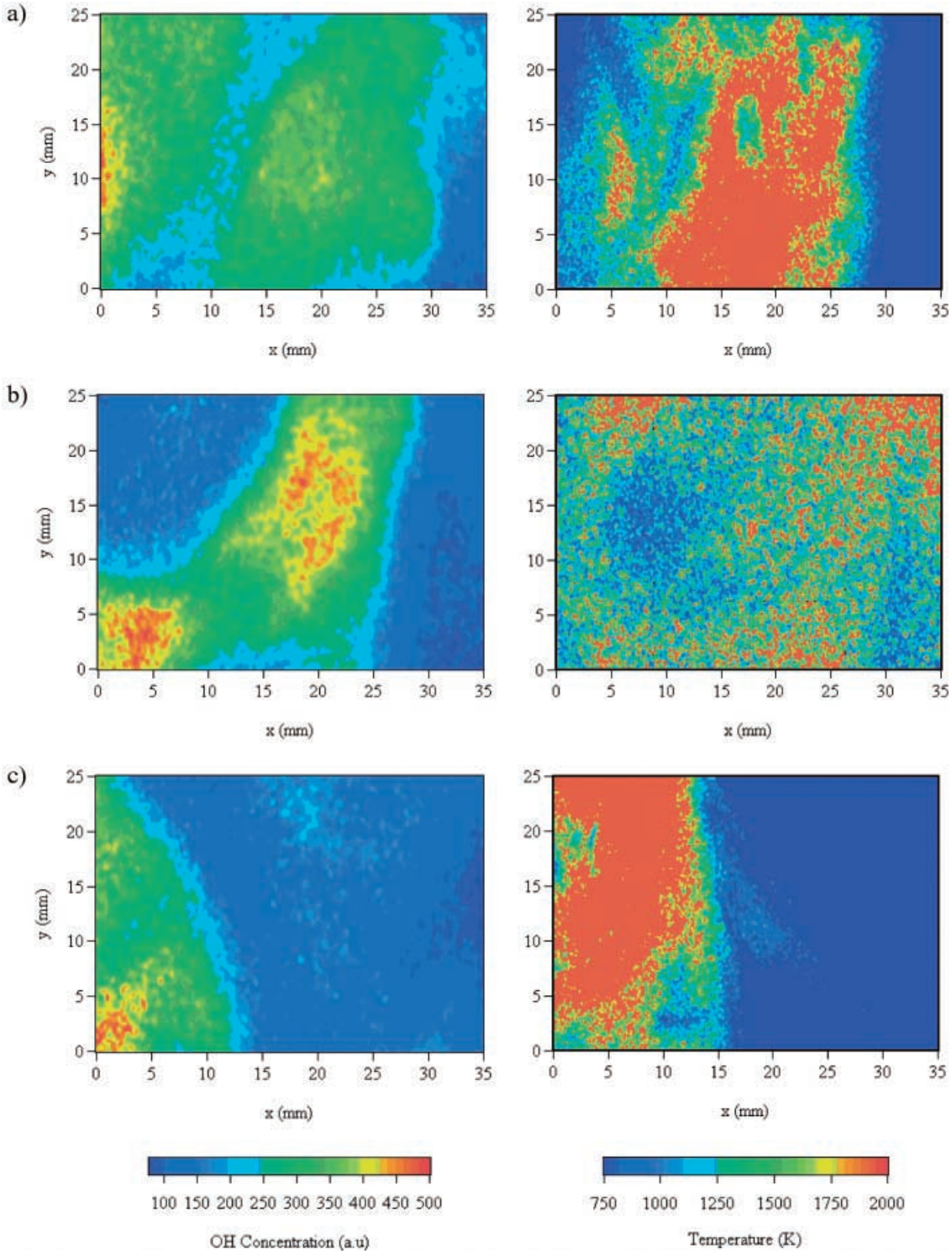

Fig. 10a–c. Instantaneous pictures of OH concentration and temperature for non-premixed combustion with $\varphi = 1.2$. **a** 5th window centered at $z = 412.5$ mm; **b** 4th window centered at $z = 312.5$ mm; **c** 3rd window centered at $z = 212.5$ mm

1993; Döbelling et al. 1996). Therefore, it is also of interest to examine if the mild combustion can be sustained with premixed mixtures. Figure 12 shows some sample pictures of instantaneous OH concentration for the equivalence ratio of 1. It is clear that there is a close resemblance to the lean non-premixed combustion (Fig. 8), in that the reaction takes place only between the second and third windows with the emission of OH radical in regions of high concentration. The similarity is due to the discrete introduction of the mixture from the six peripheral jets, which enhanced the mixing of the fresh fuel/air with the flue gases long before the reaction was initiated. Hence, when reaction started the local equivalence ratio was already lower than that at the exit.

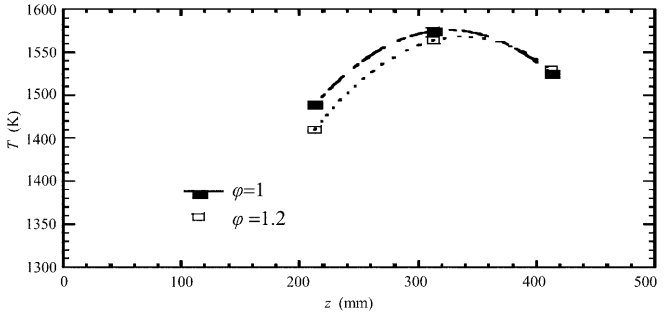

Fig. 11. Space-averaged temperature variation away from the central nozzle

4 Concluding remarks

The particulars of the aerodynamic design of the mild combustion burner such as the strong shear due to the reactants supplied from discrete jets seem crucially important for recirculating the flue gases and generating high mixing rates. In this arrangement, the entrainment in the close vicinity of the burner occurs with a Biot–Savart effect, in that the flue gases are simply inducted into the mainstream at the center, which leads to a less intermittent process and so relatively lower values of $\sqrt{\tau_2/\tau_1}$. Slightly downstream, mixing effects are enhanced with the turbulent fluctuations, and the magnitudes of the second order moments of the residence time pdf increase with respect to the mean values, which indicates an entrainment of more intermittent nature. The entrainment of this sort causes the flue gases to partially encapsulate the jets introduced from the six peripheral nozzles. When the flow attains a single-jet-like structure, the large-scale turbulent fluctuations have already formed pockets of flammable mixture surrounded by inert gases. The reaction thus initiates only away from the burner and in disconnected regions. This is confirmed in the Rayleigh pictures in that, in a small region near the centerline where the reaction initiates, strong temperature gradients prevail within the structures.

As the distance from the burner further increases, the reaction seems to follow local flow patterns, which occasionally progresses radially outwards with large structures, resulting in a clear increase in space-averaged temperature. At these locations, due to high stretching rates of the large structures, the flame is likely to be nearly extinct. However, the flue gases entrained so far increase the inert content of the fresh mixture so that chemical kinetics has also become slow enough with time scales comparable to the time scales of the flow. This provides sufficient time for mixing between the reactants and flue gases, and raises the temperature of the reactants with competing effects on ignition. As a result, the temperature rise due to mild combustion occurs significantly lower than that of a typical combustion. Avoiding temperature peaks thus suppresses the thermal NO formation.

The results also show that when the equivalence ratio is increased with non-premixed mixtures, the combustion takes place further downstream towards the roof. In the case of premixed combustion of equal equivalence ratio, however, the reaction starts and terminates earlier.

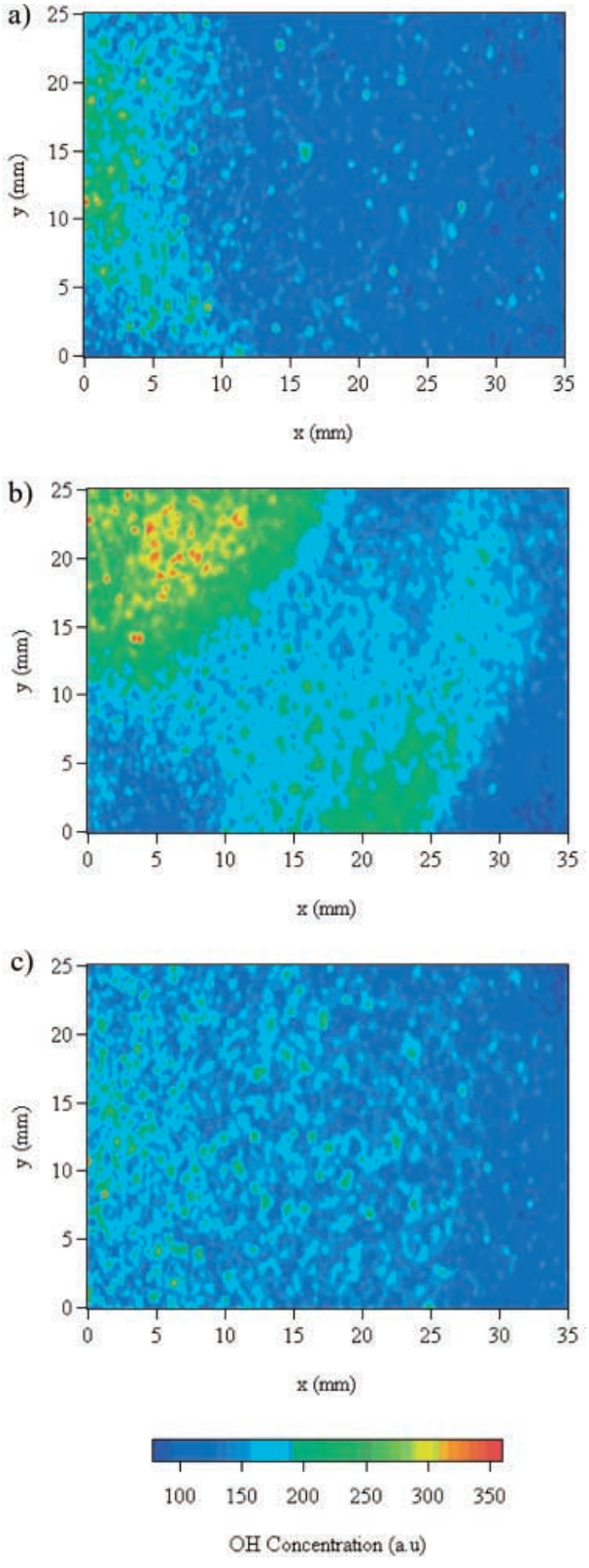

Fig. 12a–c. Instantaneous pictures of OH concentration for premixed combustion with $\varphi = 1.0$. **a** 4th window centered at $z = 312.5$ mm; **b** 3rd window centered at $z = 212.5$ mm; **c** 2nd window centered at $z = 112.5$ mm

References

Bell CT; Warren S (1983) Experience with burner NO_x reduction. Hydrocarbon Proc, September, 145–147

Bowman CT (1992) Control of combustion-generated nitrogen oxide emissions: technology driven by regulation. In: 24th (International) Symposium on Combustion, Sydney. The Combustion Institute, Pittsburg, Penn., p 859

Chomiak J; Longwell JP; Sarofim AF (1992) Combustion of low calorific value gases, problems and prospects. Prog Energy Combust Sci 15: 109–129

Coelho PJ; Peters N (2001) Numerical simulation of a mild combustion burner. Combust Flame 124: 503–518

De Joannon M; Langella G; Beretta F; Cavaliere A; Noviello C (1999) Mild combustion: process features and technological constrains. Proceedings of the Mediterranean Symposium, pp 347–360

Döbelling K; Knöpfel HP; Polifke W; Winkler D; Steinbach C; Sattelmayer T (1996) Low-NO_x premixed combustion of Mbtu fuels using the ABB double cone burner (EV burner). J Eng Gas Turbines Pwr 118: 46–53

Flamme M (1994) NO_x output from industrial burners using combustion air preheating or oxygen enrichment. Round Table Committee F, 19th World Gas Conference, Milan, June

Flamme M; Kremer H (1995) NO_x-reduction potential of high temperature processes. International Gas Research Conference, Cannes, France

Garg A (1994) Specify better low-NO_x burners for furnaces. Chem Eng Prog, January, 46–49

Hanby VI (1994) Combustion and pollution control in heating systems. Springer, Berlin Heidelberg New York

Hayhurst AN; Lawrence AD (1992) Emissions of nitrous oxide from combustion sources. Prog Energy Combust Sci 18: 529–552

Kohse-Höinghaus K (1994) Laser techniques for the quantitative detection of reactive intermediates in combustion systems. Prog Energy Combust Sci 20: 203–279

Lang W; Poinsot T; Candel S (1987) Active control of combustion instabilities. Combust Flame 70: 281–289

Long MB (1992) Multidimensional imaging in combusting flows by Lorenz–Mie, Rayleigh and Raman scattering. In: Taylor AM (ed) Combustion flow instrumentation. Academic Press, London

Long MB; Chu BT; Chang RK (1981) Instantaneous two dimensional gas concentration measurements by light scattering. AIAA J 19: 1151–1157

Mansour MS; Bilger RW; Dibble RW (1989) Raman/Rayleigh–Mie scattering measurements in a reverse flow reactor close to extinction. 22nd Symposium on Combustion. The Combustion Institute, Cambridge

Mastorakos E; Taylor AM; Whitelaw JH (1993) Turbulent counterflow flames with reactants diluted by hot products. Joint Meeting of the British and German Sections. The Combustion Institute, Cambridge

McManus KR; Poinsot T; Candel SM (1993) A review of active control of combustion instabilities. Prog Energy Combust Sci 19: 1–29

McVey JB; Padget FC; Rosfjord TJ; Hu AS; Peracchio AA; Schlein B; Tegel DR (1993) Evaluation of low-NO_x combustor concepts for aeroderivative gas turbine engines. J Eng Gas Turbines Power 115: 581–587

Milani A (1994) NO_x emissions from gas fired reheating furnaces for steelmaking plants. Round Table Committee F, 19th World Gas Conference, Milan, June

Miller JA; Bowman CT (1989) Mechanism and modeling of nitrogen chemistry in combustion. Prog Energy Combust Sci 15: 287–338

Namer I; Schefer RW (1985) Error estimates for Rayleigh scattering density and temperature measurements in premixed flames. Exp Fluids 3: 1–9

Özdemir IB; Whitelaw JH; Biçen AF (1996) Flow properties and passive scalar transport in a model room with relevance to ventilation efficiency. Proc Inst Mech Eng 210: 297–307

Perry AE; Lim TT; Chong MS (1980) The instantaneous velocity fields of coherent structures in coflowing jets and wakes. J Fluid Mech 101: 243–256

Peters N (2000) Turbulent combustion. Cambridge, Cambridge University Press, p. 4

Plessing T; Peters N; Wünning JG (1998) Laseroptical investigation of highly preheated combustion with strong exhaust gas recirculation. 28th International (International) Symposium on Combustion, Boulder, Colo. The Combustion Institue, Pittsburgh, Penn., pp 3197–3204

Saul A; Altemark D (1991) Lean-burn premixed combustion in gas turbine combustors. Gas Wärme Int 40: 336

Smart JP; Morgan DJ (1994) The effectiveness of multi-fuel reburning in an internally fuel-staged burner for NO_x reduction. Fuel 73: 1437–1442

Spliethoff H; Greul U; Rüdiger H; Hein KRG (1996) Basic effects of NO_x emissions in air-staging and reburning at a bench-scale test facility. Fuel 75: 560–564

Stepowski D (1992) Laser measurements of scalars in turbulent diffusion flames. Prog Energy Combust Sci 18: 463–491

Tanaka R (1995) New progress of energy saving technology toward the 21st century: frontier of combustion and heat transfer technology. 11th IFRF Members Conference, June

Telger R; Roth W (1995) Betriebserfahrung beim Einsatz von Brennern mit flammloser Oxidation. Gas Wärme Int 44: 332–337

Teng H; Huang T-S (1996) Control of NO_x emissions through combustion modifications for reheating furnaces in steel plants. Fuel 75: 149–156

Wood SC (1994) Select the right NO_x control technology. Chem Eng Prog, January: 32–38

Wünning JA; Wünning JG (1997) Flameless oxidation to reduce thermal NO-formation. Prog Energy Combust Sci 23: 81–94

Yanta WC (1973) Turbulence measurements with a laser Doppler velocimeter, Report NOLTR 73–94, Naval Ordinance Labs, White Oak, Silver Spring

Zabetakis MG (1965) Flammability characteristics of combustible gases and vapours. Bulletin 627, Bureau of Mines, USA

Zeldovich J (1946) The oxidation of nitrogen in combustion and explosions. Acta Physiochim URSS XXI(4)

Zhao F-Q; Hiroyasu H (1993) The applications of laser Rayleigh scattering to combustion diagnostics. Prog Energy Combust Sci 19: 447–485